

The g^0 meson observed in our data at 1680 MeV is consistent with the previously reported resonances. Our data are too limited in statistical accuracy to determine uniquely the spin of the g^0 .

ACKNOWLEDGMENTS

This experiment was made possible by the help and cooperation of the Shutt bubble chamber group and the AGS personnel of Brookhaven National Laboratory. Particular thanks are due to Dr. D. Rahm and Dr. M. Webster for their assistance with the beam. We are grateful to Dr. R. Jabbur of Argonne National Laboratory for providing helpful calculations. We wish to

acknowledge the assistance of J. B. Annable, R. J. Schlenz, and the Notre Dame scanning and measuring staff, R. Marshall, R. VanBerg, W. Kononenko, F. Forman, and the Pennsylvania scanning and measuring staff, with the data analysis. The cooperation of the Notre Dame, Pennsylvania, and New York University Computer Centers is appreciated. J. W. Andrews and J. W. Lamsa assisted in the preparation of these data. The Pennsylvania group wishes to thank Dr. V. Hagopian, Dr. H. Brody, and Dr. Y. L. Pan for their advice and help throughout this experiment. One of us (H. Y.) would like to thank the Rochester bubble chamber group, especially Dr. T. Ferbel, for helpful discussions.

Nucleon-Nucleon Polarization between 300 and 700 MeV*

DAVID CHENG AND BURNS MACDONALD†

Lawrence Radiation Laboratory, University of California, Berkeley, California

AND

JEROME A. HELLAND

University of California, Los Angeles, California

AND

PHILIP M. OGDEN

Seattle Pacific College, Seattle, Washington

(Received 23 January 1967)

The polarization parameter $P(\theta^*)$ has been measured at beam energies of 310, 400, 500, 600, and 700 MeV over the range in the c.m. scattering angles $30 \text{ deg} \leq \theta^* \leq 150 \text{ deg}$ to an accuracy of typically ± 0.03 for pn scattering, and ± 0.02 for pp scattering. A polarized proton beam was scattered from an unpolarized target—deuterium for quasifree pn and pp measurements, hydrogen for free pp measurements—and both of the outgoing nucleons from the (quasi-) elastic scatter were detected by an array of 27 scintillation counters in multichannel coincidences. It was found that $P(\theta^*)$ for pp scattering can be approximated by $A \sin\theta^* \cos\theta^*$, where A varies from -0.25 at 310 MeV to -0.4 at 700 MeV in this range. A comparison of $P(\theta^*)$ for free and quasifree pp scattering reveals good agreement between the two.

I. INTRODUCTION

NUCLEON-NUCLEON (NN) scattering amplitudes are determined experimentally by scattering experiments involving cross sections and/or polarizations. At low energies, where inelastic processes are not important, these amplitudes are conveniently parametrized at each energy and all angles by a set of real phase shifts and mixing parameters. However, at higher energies, not only do more phase shifts of higher angular momentum states contribute to the scattering, but also the phase shifts become complex because of the opening of inelastic channels. Therefore, phase-shift analysis becomes extremely difficult and impractical, and its physical significance becomes less

apparent. An alternative scheme as a meeting ground between experimental data and theoretical models has been proposed by Wolfenstein.¹ In the pp system, there are five complex (Wolfenstein¹) amplitudes which are functions of energy and c.m. angle, θ^* , ($0 \leq \theta^* \leq \pi/2$). (See Appendix.) These amplitudes have symmetry properties about $\theta^* = \pi/2$. In order that these five complex amplitudes be determined experimentally at a given energy and angle, at least nine linearly independent observables (such as differential cross section, polarization, and rotation parameters) must be measured to solve for nine of the ten real quantities in the five complex amplitudes. (One phase is arbitrary.²)

¹ L. Wolfenstein and J. Ashkin, *Phys. Rev.* **85**, 947 (1952).

² The over-all phase is not determined from this formalism because the amplitudes are bilinear in the observables. However, the phase can be determined from the optical theorem relating the imaginary part of the scattering amplitude to the total cross section.

* Work supported by the U. S. Atomic Energy Commission.

† Present address: Virginia Polytechnic Institute, Blacksburg, Virginia.

Since the experimental error for each measurement is not infinitesimal, and the equations for the observables and amplitudes are bilinear, in practice more than nine experiments must be performed in order to determine the pp scattering amplitudes uniquely.

On the other hand, when one simultaneously analyzes both the pp and pn (collectively NN) amplitudes, there are 10 complex amplitudes to be determined (5 for each isospin state), or 19 independent real numbers. (Again, one phase is arbitrary.²) On the basis of interference terms in the pp and pn amplitudes, one can obtain three equations by equating observables to amplitudes for each "set" of measurements.³ (A set contains a measurement of a pp observable at an angle θ^* , with $0 \leq \theta^* \leq \pi/2$, and pn measurements of the same observables at angles θ^* and $\pi - \theta^*$.⁴)

Thus, one can obtain 21 equations with seven sets of measurements, which, in principle, are more than sufficient to determine the NN amplitudes uniquely. These advantages are realized experimentally also, since pn and pp measurements can occasionally be performed on the same experimental setup with a change in either target nucleon or beam nucleon (or both) from proton to neutron or vice versa. With a counter hodoscope or spark chamber setup, one essentially measures the entire angular spectrum simultaneously.

II. EXPERIMENTAL METHOD AND APPARATUS

In this experiment, the pn and pp polarization parameters were measured at energies from 310 to 700 MeV, and c.m. angles from 30 to 150 deg with the same experimental setup. The polarized proton beam was produced by scattering an unpolarized external proton beam from the Berkeley 184-in. cyclotron on a carbon target at ± 6 deg. The polarization of this beam was determined by means of a second scatter on an identical carbon target and by measuring the asymmetry with a pair of counter telescopes at ± 6 deg from the second

³ B. M. Golovin, V. P. Dzhelelov, V. S. Nadezhdin, and V. I. Saturo, Zh. Eksperim. i Teor. Fiz. **36**, 433 (1959), [English transl.: Soviet Phys.—JETP **9**, 302 (1959)].

⁴ Because of the symmetries of the Wolfenstein parameters about $\theta^* = \pi/2$ and the identical particles in pp scattering, some of the observables exhibit symmetries about $\theta^* = \pi/2$, e.g.,

$$\begin{aligned} I_0(\pi - \theta^*) &= I_0(\theta^*), \\ P(\pi - \theta^*) &= -P(\theta^*), \\ C_{nn}(\pi - \theta^*) &= C_{nn}(\theta^*), \\ C_{im}(\pi - \theta^*) &= C_{im}(\theta^*). \end{aligned}$$

Some observables are related to other observables, e.g.,

$$\begin{aligned} C_{iu}(\pi - \theta^*) &= C_{mm}(\theta^*), \\ D(\pi - \theta^*) &= D_t(\theta^*), \\ R(\pi - \theta^*) &= R'_t(\theta^*), \\ A(\pi - \theta^*) &= A'_t(\theta^*), \end{aligned}$$

where the subscript t denotes transfer [See C. R. Schumacher and H. A. Bethe, Phys. Rev. **121**, 1534 (1961)], i.e., the measurement of the polarization of the recoiled particle instead of the scattered particle. In the second case, if one measures these observables at angles θ^* between 0 and π (as in the np case), one obtains two independent equations equating observables to amplitudes.

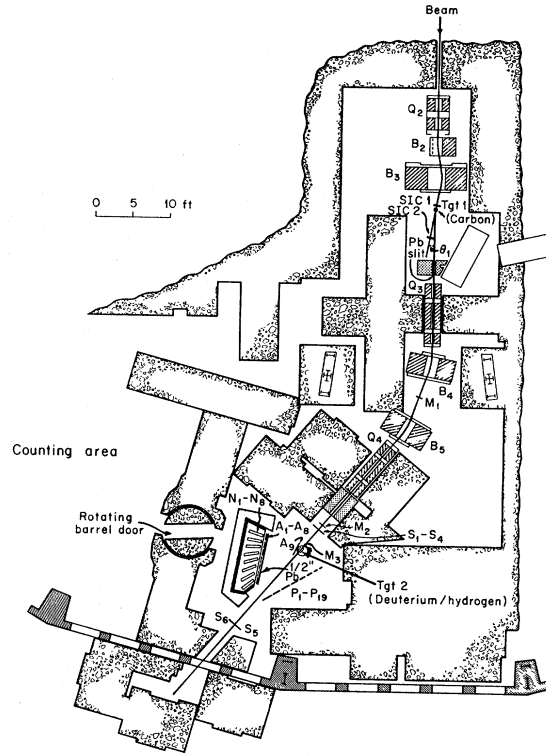


FIG. 1. Layout of the experimental setup.

target. By reversal of the first scattering angle, the beam polarization was caused to reverse sign (i.e., partial spin alignment changed from up to down or vice versa). The polarized proton beam was scattered from an unpolarized target (deuterium for quasifree pn and pp measurements, hydrogen for free pp measurements) and both of the outgoing nucleons from the (quasi-) elastic scatter were detected by an array of 27 scintillation counters in multichannel coincidences. We obtained the NN polarization by measuring, at a given angle, the asymmetry in the NN scattering due to beam polarized up and down, and then dividing this by the absolute value of the beam polarization.

The experimental setup is shown in Fig. 1. The external proton beam from the cyclotron, degraded to the desired energy with copper absorbers, entered the experimental area as shown at the top of the figure. The two bending magnets B_2 and B_3 bent the beam away from and back toward the beam line, respectively. The beam intersected the original beam line at a carbon target with an angle θ_1 . The scattered (hence polarized) protons passing through the lead defining slit were momentum analyzed [momentum spread $\Delta p/p = 6\%$ full width at half-maximum (FWHM)] and finally focused (achromatically) on the second target. Upon reversal of the fields in B_2 and B_3 , the angle θ_1 was reversed, and hence the sign of the beam polarization was also reversed. The angle θ_1 was monitored by a pair of split ion chambers; one before and one after the

polarizing target ensured that the angle θ_1 was accurate and consistent to ± 0.2 deg.

The polarized beam was monitored by three counters (M_1 , M_2 , and M_3) in coincidence. Counter M_1 was at the intermediate focus of the beam where the momentum dispersion was maximum; the spatial extent of M_1 limited the momentum dispersion of the beam accepted by the beam monitor system $M_1M_2M_3$. Counter M_3 , a thin counter close to the second target, selected beam particles going through only the central portion of the target.

The polarized proton beam was kept centered on the beam line by means of split counters S_1 to S_4 , located near M_2 . They counted the fraction of beam to the left and right of the beam line, and above and below the beam height, in coincidence with the monitor signals. Counters S_5 and S_6 were located downstream to count the left and right portion of the beam. By slight trimming of the currents in magnets B_4 and B_5 , it was possible to keep the left-right counters balanced to within 1% in both sets of split counters, thus ensuring that the beam was on the beam line.

To the left of the second target (looking downstream) were 19 scintillation counters P_1 to P_{19} . They detected charged particles (mainly scattered protons). To the right were counter A_9 , $\frac{1}{2}$ in. of lead, counters A_1 to A_8 , and eight 6-in.-thick scintillation counters N_1 to N_8 . These thick counters detected high-energy neutrons (> 5 MeV) that deflected protons in the scintillator. The efficiency of these counters⁵ was about 15%. They were also used to detect charged particles directly with unit efficiency. During pn runs, A_1 to A_9 were in anti-coincidence to veto events in which a proton or a γ ray headed toward the N counters. During pp runs, A_1 to A_8 and the $\frac{1}{2}$ in. of lead were removed, and A_9 was put in coincidence to ensure that the N counters would detect only charged particles.

The N counters were shielded on all sides except the front by layers of paraffin, boric acid, lead, and steel totaling 18 to 24 in. thick for minimizing the neutron background.

The second target was a liquid-hydrogen or liquid-deuterium target of standard LRL design with a 7.5-mil

Mylar target flask, $3\frac{3}{4}$ in. in diameter by 5 in. along the beam. Surrounding the target was a vacuum jacket with a 310-deg window of 25-mil Mylar.

The beam energy was measured by means of a telescope counter with variable thickness of copper absorbers in the beam. The energies,⁶ normalized for the center of the second target, and widths corrected for range straggling⁷ [energy spreads in half-width at half-maximum (HWHM)] are tabulated in Table I. The approximate beam-intensity ratios at the second target due to beam loss through degrading are also listed.

An event was defined by a coincidence of the monitor counters $M_1M_2M_3=M$, at least one P counter, at least one N counter, and no anticounter. This system either detected two charged particles (predominantly pp), or one charged and one neutral particle (predominantly pn) in the final state. The count from the particular P and N counters that fired for each event were recorded on a magnetic tape through an on-line PDP-5 computer. Six types of runs were made at each energy for both pp and pn systems: with deuterium (D), hydrogen (H), and empty flask (B_B) targets, each with both signs of beam polarization. Thus, there was a total of 12 different types of runs at each energy.

The three different target conditions in the pn runs were used for background elimination. The three in the pp runs were for comparison of pp runs in a free and quasifree proton target.

TABLE I. Beam energies and intensities at the center of the second target.

Beam (MeV)	Measured energy* (MeV)	Cu degrader thickness (in.)	Approximate intensity ratio ^b
310	307 ± 11	$8\frac{1}{8}$	0.0022
400	394 ± 12	$7\frac{1}{4}$	0.0035
500	498 ± 11	$5\frac{1}{8}$	0.0046
600	601 ± 9	$2\frac{7}{8}$	0.0071
700	702 ± 5	0	1.0000

* The beam value is known to approximately 3 MeV. The listed spreads represent half-width at half-maximum.

^b For explanation, see text.

⁵ R. J. Kurz, Lawrence Radiation Laboratory Report No. UCRL-11339, 1964 (unpublished).

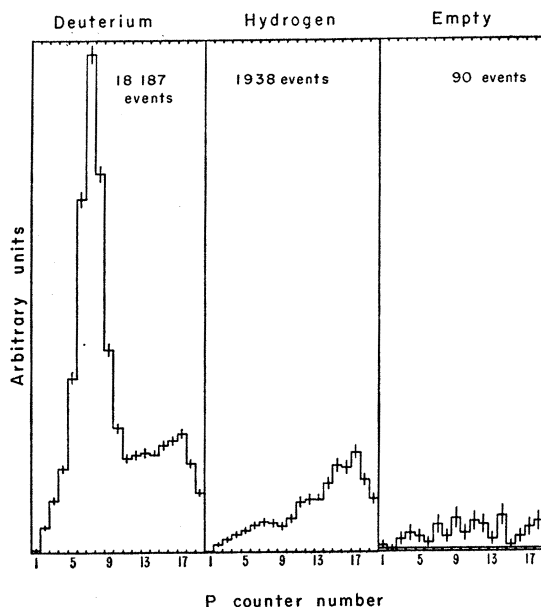


FIG. 2. Comparison of pn events in all proton counters for neutron counter N_8 at 700-MeV incident proton energy for three different target conditions: target filled with liquid deuterium, target filled with liquid hydrogen, and target empty. Horizontal line indicates position of zero counts.

⁶ W. A. Aron, B. G. Hoffman, and F. C. Williams, Lawrence Radiation Laboratory Report No. UCRL-121, 1949 (unpublished).

⁷ R. M. Sternheimer, Phys. Rev. **117**, 485 (1959).

TABLE II. Background contribution from $NN \rightarrow NN\pi$ in liquid H_2 and liquid D_2 targets.

Target	Process	Final state		Total cross section (mb) at following energies (MeV)			
		1 neutron + 1 charged particle	2 charged particles	400	500	600	700
D,H	$pp \rightarrow pp\pi^0$		X	0.06	0.5	2.0	4.0
D,H	$pp \rightarrow pn\pi^+$	X	X	0.4	3.5	7.0	12.0
D	$pn \rightarrow pn\pi^0$	X		0.2	1.5	2.5	4.0
D	$pn \rightarrow pp\pi^-$		X	0.03	0.3	1.0	2.0
D	$pn \rightarrow nn\pi^+$	X		0.03	0.3	1.0	2.0
Summary for pn		$\sum H$		0.4	3.5	7.0	12.0
		$\sum D$		0.63	5.3	10.5	18.0
		$\sum D/\sum H$		1.6	1.5	1.5	1.5
Summary for pp			$\sum H$	0.46	4.0	9.0	16.0
			$\sum D$	0.49	4.3	10.0	18.0
			$\sum D/\sum H$	1.1	1.1	1.1	1.1

III. ANALYSIS AND RESULTS

The events of a specific type with only one P and one N counter counting were combined to form a 19×8 array $M(P_i, N_j)$, where M is the number of counts per monitor count in the channel (P_i, N_j) , $i=1, \dots, 19$, and $j=1, \dots, 8$. Typical distributions for pn and pp runs at 700 MeV are plotted in Figs. 2 and 3, respectively, for counter N_3 . The main peak on the left represents elastic (or quasi-elastic) pn or pp events. The rest is background.

For the pp runs in hydrogen, the "pure" pp events were obtained by making the subtraction $H - B_E - B_{E'}$, where B_E represents the background due to the empty target, and $B_{E'}$ (extrapolation) is the additional back-

ground from inelastic events (see Fig. 3). The background $B_{E'}$ was determined by starting with the curve from $H - B_E$ and subtracting a sufficient number of events from each of the three channels forming the main peak so as to be left with a smooth curve across those three channels and the three channels on each side.

For the pn and pp runs in deuterium, the quasi-elastic peaks have long tails in which backgrounds (mainly pion production) and NN events overlap. We have used the hydrogen-target runs to determine the background contribution from the proton, and to estimate the additional contribution to background from the neutron in the deuterium target. In Table II, we have summarized the particular $NN \rightarrow NN\pi$ processes (in which

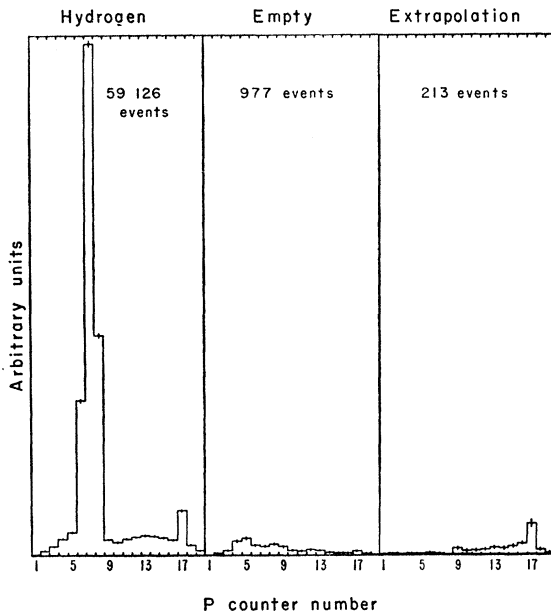


FIG. 3. Comparison of pp events in all proton counters for neutron counter N_3 at 700-MeV incident proton energy for two different target conditions: target filled with liquid hydrogen, target empty, and background extrapolation from off-center peak events under target filled minus target empty.

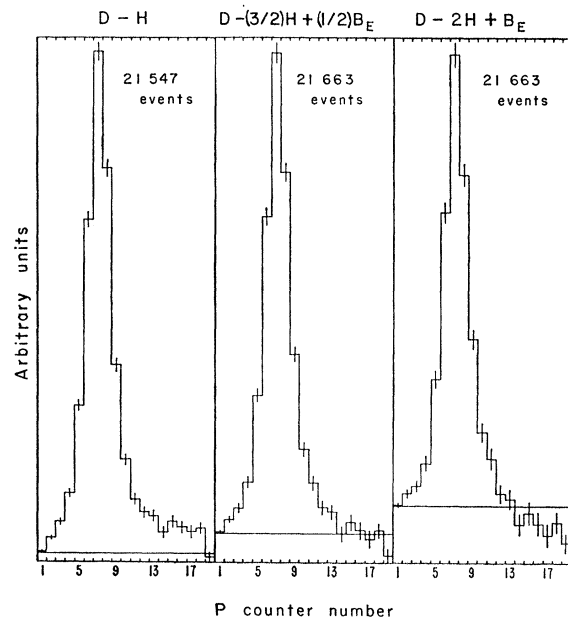


FIG. 4. Comparison of pn events in all proton counters for N_3 at 700-MeV incident proton energy for different methods of background subtraction (see text). Horizontal lines indicate position of zero counts.

only two particles are detected by the counters) that can be confused with one-proton or one-neutron events. Weighting the contribution of each interaction by its total cross section,⁸ one finds that for pn runs, elimination of the background requires the combination of $D-\frac{3}{2}H+\frac{1}{2}B_E$. For pp runs with a deuterium target, $D-B_E-B_{E'}$ is required, where $B_{E'}$ is the same B_E as was determined for hydrogen-target runs. Figure 4 shows three different combinations for pn runs at 700 MeV with a deuterium. The chosen combination ($D-\frac{3}{2}H+\frac{1}{2}B_E$) is clearly favored. Since the background is very small, the maximum difference of various combinations is only a 2% effect on the asymmetry calculation.

The two-body background reactions in pp interactions, such as $pd \rightarrow pd$ or $pp \rightarrow \pi^+d$, have very negligible cross sections and most of them do not overlap with the elastic peak. There is no background contribution in pn interactions from two-body final states.

After the above-mentioned background corrections were applied, the three bins with the maximum number of events were summed, and the asymmetry was calculated. Histograms for 700-MeV pn (deuterium) and pp (hydrogen) runs in counter N_8 are shown in Figs. 5 and 6, respectively. In each figure, the histogram on the right is the Monte Carlo calculated distribution with the input of experimental condition of the beam, target, and counter information. With pn runs, the target

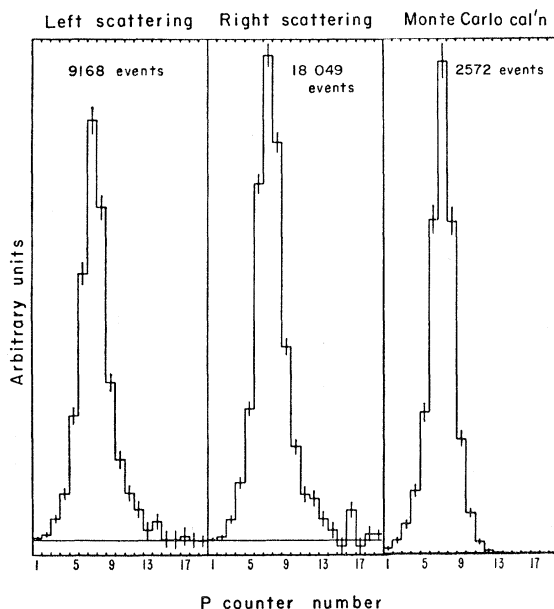


FIG. 5. Comparison of pn events in proton counters for neutron counter N_8 at 700-MeV incident proton energy for beam polarization up and down, and Monte Carlo calculation simulation of this experiment, assuming the target neutron is moving with just the Hulthén momentum distribution (see text). Horizontal lines indicate position of zero counts.

⁸ W. O. Lock, *High Energy Nuclear Physics* (John Wiley & Sons, Inc., New York, 1960), Chap. VIII, pp. 161-179.

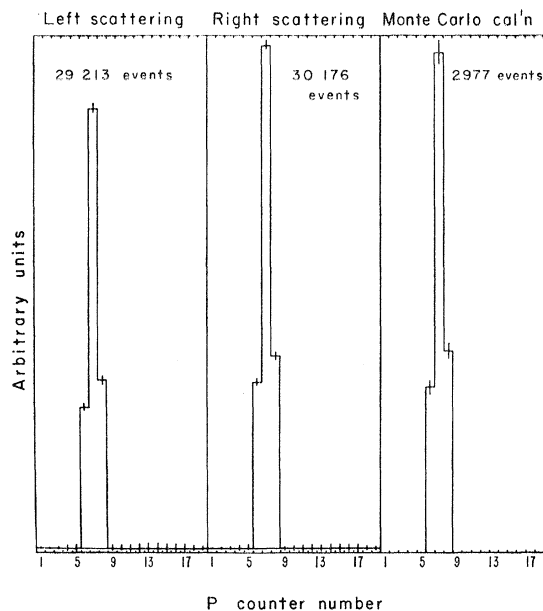


FIG. 6. Comparison of pp events in proton counters for neutron counter N_8 at 700-MeV incident proton energy for beam polarization up and down, and Monte Carlo calculation simulation of this experiment, assuming the target proton is moving with just the Hulthén momentum distribution (see text). Horizontal lines indicate position of zero counts.

neutron is approximated by a "free" neutron moving with a Hulthén distribution.⁹ For pp runs (Fig. 6), the Monte Carlo distribution agrees in shape with the measured distribution. The pn Monte Carlo distribution (Fig. 5) is shifted slightly to the left of the experimental distribution; this may be due to the off-mass-shell effect of the target nucleon, or the binding effect of the spectator proton.

Because of the finite angular acceptance of the first scattering angle by the slit, the beam spot at the final target was not symmetrical in either spatial or angular distribution. This lack of symmetry is caused by the sharp forward peaking of the angular distribution of the proton in pC scattering. For example, at 725 MeV the data of McManigal *et al.*¹⁰ indicate that the differential cross section at 7 deg is twice that at 5 deg. The spatial and angular distribution of the beam at the final target were not measured in this experiment. By assuming the worst possible conditions and making Monte Carlo calculations,¹¹ one can place an upper limit on the false scattering asymmetries arising from beam asymmetries. The maximum error in the scattering asymmetry from these calculations is about 10% in N_1 and N_8 for pp , about 5% in N_8 for pn , and negligible for all the other channels.

⁹ L. Hulthén and M. Sugawara, *Encyclopedia of Physics* (Springer-Verlag, Berlin, 1957), Vol. 39.

¹⁰ P. G. McManigal, R. D. Eandi, S. N. Kaplan, and B. J. Moyer, *Phys. Rev.* **137**, B620 (1965).

¹¹ For more details, see D. Cheng, Lawrence Radiation Laboratory Report No. UCRL-11926, 1965 (unpublished).

The beam polarization was determined¹¹ to within $\pm 3\%$. This uncertainty is the uncertainty in over-all normalization.

Other sources of error were minimized. For example, the contribution to the error from random coincidences and anticoincidences was $< 1\%$ because the beam was maintained at a relatively low and constant level.¹¹ The contribution to the error from the movement of the beam was essentially eliminated by keeping the beam centered on both targets throughout the whole run.

The asymmetry and polarization for each neutron counter were calculated in the usual manner. The asymmetry is given by the expression $\epsilon(N) = [L(N) - R(N)] / [L(N) + R(N)]$, where N is a given neutron counter, and $L(N)$ [$R(N)$] is the number of background sub-

TABLE III. Polarization parameters in the pn system. (Over-all normalization uncertainty is $< 3\%$. Errors shown are due to statistics only.) θ^* = proton scattering angle in c.m. system; ϵ = asymmetry; P = polarization.

Beam energy and polarization	θ^* (deg) ^a	$\epsilon(\%)$	P	
700 MeV, $P_B = 0.274$	29.5 \pm 6.7	9.15 \pm 0.75	0.334 \pm 0.027	
	44.3 \pm 6.7	8.36 \pm 0.46	0.305 \pm 0.017	
	60.4 \pm 6.5	4.29 \pm 0.91	0.157 \pm 0.033	
	77.1 \pm 6.0	-1.86 \pm 0.81	-0.068 \pm 0.030	
	93.8 \pm 5.7	-9.65 \pm 0.72	-0.352 \pm 0.026	
	110.9 \pm 5.4	-11.27 \pm 0.87	-0.411 \pm 0.032	
	127.1 \pm 5.3	-6.78 \pm 0.53	-0.247 \pm 0.019	
	143.2 \pm 4.9	-3.99 \pm 0.52	-0.146 \pm 0.019	
	600 MeV, $P_B = 0.316$	33.0 \pm 6.0	11.49 \pm 1.26	0.364 \pm 0.040
		48.5 \pm 5.8	7.92 \pm 1.30	0.251 \pm 0.041
64.8 \pm 5.6		2.67 \pm 0.96	0.084 \pm 0.030	
81.3 \pm 5.7		-4.90 \pm 0.88	-0.155 \pm 0.028	
97.8 \pm 5.6		-9.95 \pm 0.99	-0.315 \pm 0.031	
114.7 \pm 5.6		-10.89 \pm 0.96	-0.345 \pm 0.030	
130.5 \pm 5.6		-7.61 \pm 0.74	-0.241 \pm 0.023	
145.6 \pm 5.1		-2.85 \pm 0.73	-0.090 \pm 0.023	
500 MeV, $P_B = 0.345$		33.4 \pm 5.8	10.23 \pm 0.82	0.297 \pm 0.024
		48.5 \pm 6.1	8.79 \pm 0.54	0.255 \pm 0.016
	64.7 \pm 5.9	3.11 \pm 0.57	0.090 \pm 0.017	
	81.2 \pm 5.9	-5.35 \pm 0.60	-0.155 \pm 0.017	
	97.9 \pm 5.9	-9.11 \pm 0.62	-0.264 \pm 0.018	
	115.0 \pm 5.9	-9.08 \pm 0.60	-0.263 \pm 0.017	
	130.9 \pm 5.7	-5.06 \pm 0.59	-0.147 \pm 0.017	
	145.2 \pm 4.9	-3.82 \pm 0.60	-0.111 \pm 0.017	
	400 MeV, $P_B = 0.382$	33.1 \pm 6.9	15.70 \pm 3.31	0.411 \pm 0.087
		48.3 \pm 6.9	10.10 \pm 0.86	0.264 \pm 0.023
66.6 \pm 7.2		3.18 \pm 1.24	0.083 \pm 0.032	
83.1 \pm 7.0		-5.80 \pm 0.98	-0.152 \pm 0.026	
99.7 \pm 6.8		-11.82 \pm 0.94	-0.309 \pm 0.025	
116.5 \pm 6.6		-10.40 \pm 0.83	-0.272 \pm 0.022	
131.1 \pm 5.9		-6.02 \pm 0.69	-0.158 \pm 0.018	
144.3 \pm 5.1		-3.97 \pm 2.14	-0.104 \pm 0.056	
310 MeV, $P_B = 0.428$		33.1 \pm 6.7	18.00 \pm 1.61	0.421 \pm 0.038
		47.8 \pm 7.2	12.27 \pm 1.11	0.287 \pm 0.026
	66.7 \pm 8.1	3.96 \pm 0.85	0.093 \pm 0.020	
	83.2 \pm 8.0	-4.87 \pm 1.02	-0.114 \pm 0.024	
	99.8 \pm 7.8	-10.22 \pm 0.80	-0.239 \pm 0.019	
	116.5 \pm 7.6	-9.31 \pm 0.69	-0.218 \pm 0.016	
	130.7 \pm 6.8	-7.45 \pm 0.75	-0.174 \pm 0.018	
	141.5 \pm 7.2	-5.68 \pm 1.32	-0.133 \pm 0.031	

^a The listed spreads represent half-width at half-maximum.

TABLE IV. pp polarization in (a) liquid H_2 and (b) liquid D_2 targets. (Over-all normalization uncertainty is less than 3% . Errors shown are due to statistics only.)

Beam energy and polarization	θ^* (deg)	$\epsilon(\%)$	P	$P/\sin\theta^*$	
(a) Liquid hydrogen					
700 MeV, $P_B = 0.274$	30.8 \pm 1.7	15.2 \pm 0.52	0.555 \pm 0.019	1.083 \pm 0.037	
	35.7 \pm 1.7	14.3 \pm 0.33	0.522 \pm 0.012	0.894 \pm 0.021	
	43.2 \pm 3.5	15.3 \pm 0.44	0.558 \pm 0.016	0.816 \pm 0.023	
	52.4 \pm 3.1	14.5 \pm 0.61	0.529 \pm 0.022	0.668 \pm 0.028	
	60.1 \pm 3.6	13.0 \pm 0.30	0.474 \pm 0.011	0.547 \pm 0.013	
	68.7 \pm 3.3	9.7 \pm 1.08	0.354 \pm 0.039	0.380 \pm 0.042	
	77.0 \pm 3.6	7.0 \pm 0.42	0.255 \pm 0.015	0.262 \pm 0.016	
	86.1 \pm 3.5	3.0 \pm 1.04	0.109 \pm 0.038	0.110 \pm 0.038	
600 MeV, $P_B = 0.316$	33.6 \pm 2.5	16.2 \pm 0.31	0.513 \pm 0.010	0.926 \pm 0.013	
	34.5 \pm 1.5	18.8 \pm 1.10	0.595 \pm 0.035	1.059 \pm 0.061	
	46.1 \pm 3.6	16.3 \pm 0.32	0.516 \pm 0.010	0.716 \pm 0.014	
	49.5 \pm 3.2	15.3 \pm 0.32	0.484 \pm 0.010	0.637 \pm 0.013	
	63.1 \pm 3.6	12.6 \pm 0.61	0.399 \pm 0.019	0.446 \pm 0.022	
	65.6 \pm 3.4	11.4 \pm 1.20	0.361 \pm 0.038	0.396 \pm 0.042	
	80.2 \pm 3.6	5.3 \pm 0.32	0.168 \pm 0.010	0.170 \pm 0.010	
	82.9 \pm 3.5	3.6 \pm 0.79	0.114 \pm 0.025	0.115 \pm 0.025	
	500 MeV, $P_B = 0.345$	33.7 \pm 2.3	16.9 \pm 0.38	0.490 \pm 0.011	0.883 \pm 0.020
		36.8 \pm 1.0	17.6 \pm 2.03	0.510 \pm 0.059	0.852 \pm 0.098
46.9 \pm 3.6		15.9 \pm 0.61	0.461 \pm 0.018	0.631 \pm 0.024	
48.7 \pm 3.1		15.6 \pm 0.49	0.452 \pm 0.014	0.602 \pm 0.019	
64.1 \pm 3.6		9.3 \pm 0.35	0.270 \pm 0.010	0.300 \pm 0.011	
64.6 \pm 3.3		10.8 \pm 0.87	0.313 \pm 0.025	0.347 \pm 0.028	
81.3 \pm 3.6		3.7 \pm 0.52	0.107 \pm 0.015	0.108 \pm 0.015	
81.8 \pm 3.5		3.9 \pm 0.55	0.113 \pm 0.016	0.114 \pm 0.016	
400 MeV, $P_B = 0.382$		33.8 \pm 2.3	16.9 \pm 0.52	0.442 \pm 0.014	0.795 \pm 0.024
		47.8 \pm 3.1	16.0 \pm 0.29	0.419 \pm 0.008	0.565 \pm 0.010
	48.0 \pm 3.6	16.0 \pm 0.41	0.419 \pm 0.011	0.564 \pm 0.014	
	63.5 \pm 3.3	10.5 \pm 0.30	0.275 \pm 0.008	0.307 \pm 0.009	
	65.2 \pm 3.7	10.4 \pm 0.37	0.272 \pm 0.010	0.300 \pm 0.011	
	80.6 \pm 3.5	4.0 \pm 0.32	0.105 \pm 0.008	0.106 \pm 0.008	
	82.5 \pm 3.7	3.2 \pm 0.33	0.084 \pm 0.009	0.084 \pm 0.009	
	310 MeV, $P_B = 0.428$	33.6 \pm 2.4	17.2 \pm 1.05	0.402 \pm 0.025	0.726 \pm 0.044
		47.3 \pm 2.8	16.0 \pm 0.31	0.374 \pm 0.007	0.509 \pm 0.010
		50.1 \pm 2.7	15.5 \pm 0.49	0.362 \pm 0.011	0.472 \pm 0.015
62.4 \pm 3.2		11.8 \pm 0.30	0.276 \pm 0.007	0.311 \pm 0.008	
66.3 \pm 3.7		9.3 \pm 0.35	0.217 \pm 0.008	0.237 \pm 0.009	
79.4 \pm 3.5		5.0 \pm 0.30	0.117 \pm 0.007	0.119 \pm 0.007	
83.7 \pm 3.6		1.5 \pm 0.35	0.035 \pm 0.008	0.035 \pm 0.008	
(b) Liquid deuterium					
700 MeV, $P_B = 0.274$		29.5 \pm 6.7	11.6 \pm 1.41	0.423 \pm 0.051	0.860 \pm 0.105
		36.8 \pm 4.9	13.4 \pm 0.88	0.489 \pm 0.032	0.816 \pm 0.054
	44.3 \pm 6.7	14.7 \pm 0.67	0.536 \pm 0.024	0.768 \pm 0.035	
	52.9 \pm 5.2	13.7 \pm 0.05	0.500 \pm 0.018	0.627 \pm 0.023	
	60.4 \pm 6.5	11.7 \pm 0.76	0.427 \pm 0.028	0.491 \pm 0.032	
	69.1 \pm 5.4	11.5 \pm 0.73	0.420 \pm 0.027	0.449 \pm 0.029	
	77.1 \pm 6.0	6.2 \pm 0.76	0.266 \pm 0.028	0.232 \pm 0.028	
	86.2 \pm 5.7	3.5 \pm 0.99	0.128 \pm 0.036	0.128 \pm 0.036	
600 MeV, $P_B = 0.316$	33.0 \pm 6.0	16.9 \pm 2.45	0.535 \pm 0.078	0.982 \pm 0.142	
	34.4 \pm 5.1	15.0 \pm 1.29	0.475 \pm 0.041	0.840 \pm 0.072	
	48.3 \pm 5.8	17.6 \pm 1.26	0.557 \pm 0.040	0.744 \pm 0.053	
	49.5 \pm 5.6	14.2 \pm 0.67	0.449 \pm 0.021	0.591 \pm 0.028	
	64.8 \pm 5.6	11.8 \pm 0.91	0.379 \pm 0.029	0.413 \pm 0.032	
	65.3 \pm 5.6	10.6 \pm 0.32	0.335 \pm 0.010	0.369 \pm 0.011	
	81.3 \pm 5.7	3.9 \pm 0.85	0.123 \pm 0.027	0.125 \pm 0.027	
	82.2 \pm 5.6	4.5 \pm 0.82	0.142 \pm 0.026	0.144 \pm 0.026	
	500 MeV, $P_B = 0.345$	33.4 \pm 5.8	17.5 \pm 2.31	0.507 \pm 0.067	0.921 \pm 0.122
		48.5 \pm 6.1	14.7 \pm 1.16	0.426 \pm 0.034	0.569 \pm 0.045
49.1 \pm 5.7		14.2 \pm 0.73	0.412 \pm 0.021	0.545 \pm 0.028	
64.7 \pm 5.9		9.1 \pm 0.78	0.264 \pm 0.023	0.292 \pm 0.025	
65.0 \pm 5.9		9.5 \pm 0.68	0.275 \pm 0.020	0.304 \pm 0.022	
81.2 \pm 5.9		4.0 \pm 0.74	0.116 \pm 0.021	0.117 \pm 0.022	
82.1 \pm 5.1		3.8 \pm 0.71	0.110 \pm 0.021	0.111 \pm 0.021	
400 MeV, $P_B = 0.382$		33.1 \pm 6.9	16.9 \pm 2.96	0.442 \pm 0.007	0.810 \pm 0.142
		48.3 \pm 6.9	14.8 \pm 1.00	0.387 \pm 0.026	0.519 \pm 0.035
		48.9 \pm 6.9	16.0 \pm 0.61	0.419 \pm 0.016	0.556 \pm 0.021
	63.5 \pm 6.6	9.4 \pm 0.58	0.246 \pm 0.015	0.275 \pm 0.017	
	66.6 \pm 7.2	10.3 \pm 0.74	0.270 \pm 0.019	0.294 \pm 0.021	
	80.3 \pm 6.8	2.9 \pm 0.59	0.076 \pm 0.015	0.077 \pm 0.016	
	83.1 \pm 7.0	2.4 \pm 0.62	0.063 \pm 0.016	0.063 \pm 0.016	

tracted counts mentioned earlier in this section for the first scatter to the left [right]. The polarization for neutron counter N is $P(N) = \epsilon(N)/P_B$, where P_B equals the beam polarization measured in this experiment (described in Sec. II).

Since each neutron counter is located at a fixed laboratory angle, its corresponding c.m. angle and

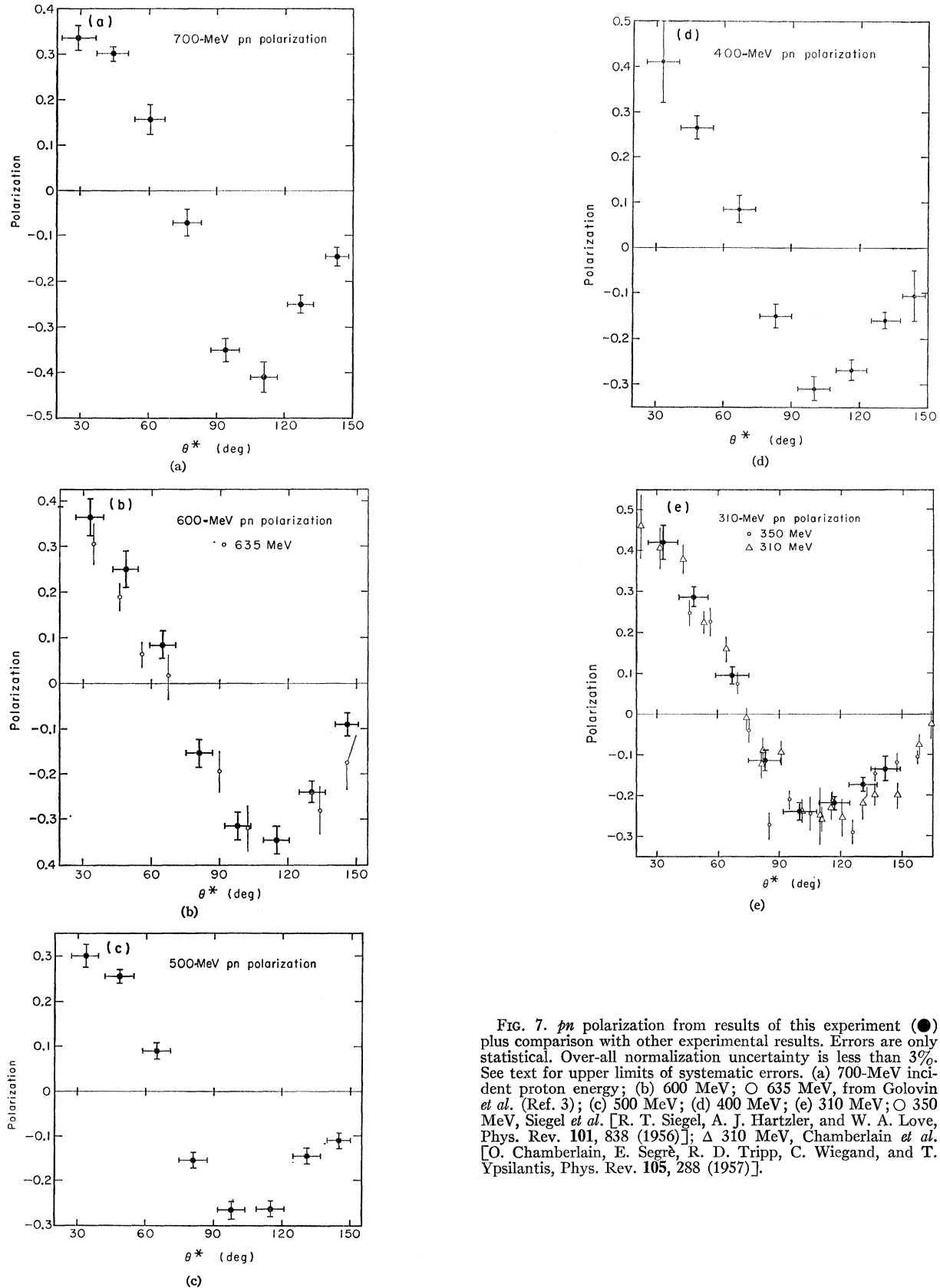


FIG. 7. pn polarization from results of this experiment (●) plus comparison with other experimental results. Errors are only statistical. Over-all normalization uncertainty is less than 3%. See text for upper limits of systematic errors. (a) 700-MeV incident proton energy; (b) 600 MeV; ○ 635 MeV, from Golovin *et al.* (Ref. 3); (c) 500 MeV; (d) 400 MeV; (e) 310 MeV; ○ 350 MeV, Siegel *et al.* [R. T. Siegel, A. J. Hartzler, and W. A. Love, *Phys. Rev.* **101**, 838 (1956)]; △ 310 MeV, Chamberlain *et al.* [O. Chamberlain, E. Segrè, R. D. Tripp, C. Wiegand, and T. Ypsilantis, *Phys. Rev.* **105**, 288 (1957)].

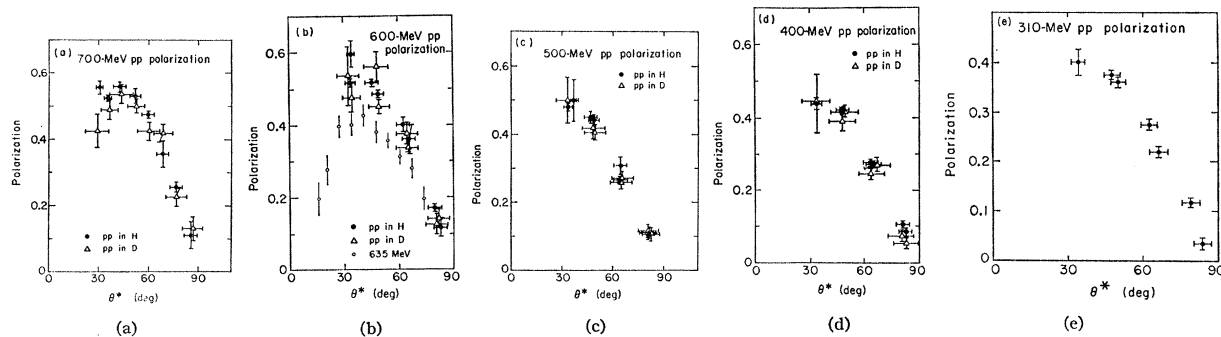


FIG. 8. pp polarizations from results of this experiment plus (\bullet) data taken with hydrogen target, Δ data taken with deuterium target plus comparisons with other experimental results that do not agree with this experiment. Errors are statistical. Over-all normalization uncertainty is less than 3%. See text for upper limits of systematic errors. (a) 700-MeV incident proton energy; (b) 600 MeV; \circ 635 MeV, Meshcheryakov *et al.* {M. G. Meshcheryakov, S. B. Nurshev, and G. D. Stoletov, Zh. Eksperim. i Teor. Fiz. 33, 37 (1957) [English transl.: Soviet Phys.—JETP 6, 28 (1958)]}; (c) 500 MeV; (d) 400 MeV; (e) 310 MeV.

spread in FWHM is calculated by the Monte Carlo method mentioned previously. For pp calculations, since $P(\theta^*)$ is antisymmetrical about $\theta^* = \pi/2$, the data for those neutron counters (i.e., $N \geq 5$) corresponding to $\theta^* > \pi/2$ have been altered in the following way. The angle has been changed to its complementary angle (i.e., $\theta^* \rightarrow \pi - \theta^*$) and the sign of polarization reversed.

Polarization parameters for pn and pp runs are tabulated in Tables III and IV; comparison between the free and quasifree pp results reveals good agreement except for forward directions where systematic errors are larger. These parameters are plotted in Fig. 7 and 8. Also plotted in Fig. 7 are previous measurements of pn and np results in this region, and in Fig. 8 are previous measurements of pp results that do not agree with this experiment.

IV. DISCUSSION

It is interesting to observe that the energy dependence of the NN polarization parameter $P^{NN}(\theta^*)$ is small and linear for pn and nearly linear for pp scatter-

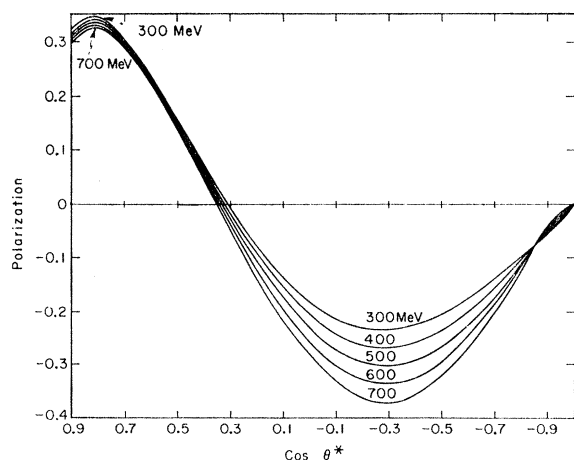


FIG. 9. Fitted curves of pn polarizations from results of this experiment. Note that only small and linear energy dependence is present.

ing (Figs. 9 and 10). Thus it is possible to parametrize the NN polarization data in the following simple form:

$$P^{NN}(\theta^*, E) = \sin\theta^* \sum_{n,l} \alpha_{nl} E^n P_l(\cos\theta^*),$$

where E is the beam kinetic energy (in BeV), θ^* is the c.m. scattering angle, and P_l is the Legendre polynomial. For our results the parameters α_{nl} are as follows:

(1) pn results: number of degrees of freedom (d) = 32 and $(\chi^2/d)^{1/2} = 1.19$.

$$\begin{aligned} \alpha_{00} &= 0.074 \pm 0.023, & \alpha_{10} &= -0.172 \pm 0.043, \\ \alpha_{01} &= 0.437 \pm 0.062, & \alpha_{11} &= 0.056 \pm 0.112, \\ \alpha_{02} &= 0.356 \pm 0.066, & \alpha_{12} &= 0.164 \pm 0.124, \\ \alpha_{03} &= 0.114 \pm 0.092, & \alpha_{13} &= -0.256 \pm 0.175. \end{aligned}$$

(2) pp results: data for both pp in (H_2) and pp in (D_2).

$$d = 59, \quad (\chi^2/d)^{1/2} = 1.28$$

$$\begin{aligned} \alpha_{01} &= 0.295 \pm 0.283, & \alpha_{11} &= 1.971 \pm 1.104, \\ \alpha_{03} &= -0.543 \pm 0.438, & \alpha_{13} &= 3.283 \pm 1.733, \\ \alpha_{05} &= -0.002 \pm 0.328, & \alpha_{15} &= -0.196 \pm 1.359, \\ \alpha_{21} &= 1.033 \pm 1.040, \\ \alpha_{23} &= -3.347 \pm 1.649, \\ \alpha_{25} &= 0.534 \pm 1.342. \end{aligned}$$

The plots for the fitted results are shown in Figs. 9 and 10.

Although the pn differential cross section I_0^{pn} is known at only a few energies in this region, it is possible to get some $I=0$, I_0 , and P results from the pp and pn data in existence, by means of the following formulas:

$$\begin{aligned} I_0^{I=0}(\theta^*) &= 2[I_0^{pn}(\theta^*) + I_0^{pn}(\pi - \theta^*)] - I_0^{pp}(\theta^*), \\ I_0 P^{I=0}(\theta^*) &= 2[I_0 P^{pn}(\theta^*) - I_0 P^{pn}(\pi - \theta^*)] - I_0 P^{pp}(\theta^*), \\ P^{I=0}(\theta^*) &= I_0 P^{I=0}(\theta^*) / I_0^{I=0}(\theta^*), \end{aligned}$$

where $0 \leq \theta^* \leq \pi/2$.

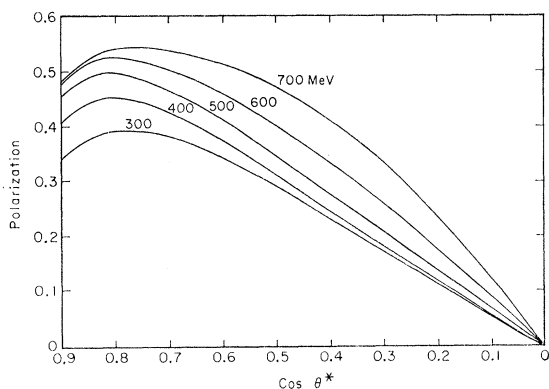


FIG. 10. Fitted curves of pp polarizations from results of this experiment. Note that only small and linear energy dependence is present.

The angular distributions of $I_0^{I=0}$ and $P^{I=0}$ versus $\cos\theta^*$ for 350, 500, and 630 MeV at which the np differential cross sections have been measured⁷ are shown in Fig. 11.¹²

Because seven "sets" (see Sec. I) of pp and pn parameters are required to determine the nucleon-nucleon scattering amplitudes, these data represent only a partial contribution toward the determination of these amplitudes. However, the results of this experiment show that the deuteron can be used as a good

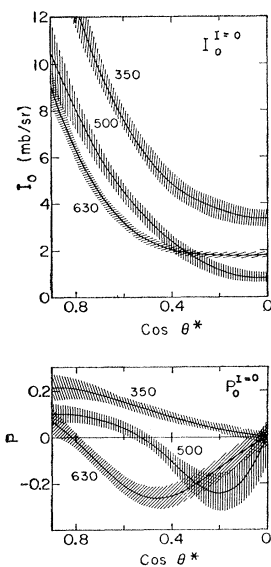


FIG. 11. Differential cross sections and polarization results for isospin=0 NN states at 350, 500, and 630 MeV.

¹² The data at 350, 500, and 630 MeV are extrapolated from np I_0 measurements to nearby energies both higher and lower. These data were taken from the reference list of the appendix of Richard Wilson's book on *The Nucleon-Nucleon Interaction* (Interscience Publishers, Inc., New York, 1963).

neutron target at high energies, provided some precautions are taken. Furthermore, since this experiment shows that the pn polarization is quite large at these energies, it should be possible to perform the more difficult triple-scattering experiments in the pn system, and the measurement of the D , R , and R' parameters for both pp and pn systems has been scheduled for the 184-in. cyclotron in the near future.

ACKNOWLEDGMENTS

We are greatly indebted to Professor B. J. Moyer and Professor A. C. Helmholz and other members of their research group for assistance in this experiment. The assistance from other sections of the Lawrence Radiation Laboratory, such as the electronics groups, the computer center staff, and the 184-in. cyclotron crew, is greatly appreciated also. Of special note is the help received from William P. Oliver, Narendra Sehgal, and Kenneth Caproni in the running of the experiment.

APPENDIX

The scattering matrix for the two-nucleon system, when spatial rotational invariance, parity conservation, time reversal invariance, and charge independence are assumed, can be written as¹

$$M = a + ic(\sigma_{1n} + \sigma_{2n}) + m\sigma_{1n}\sigma_{2n} + (g+h)\sigma_{1l}\sigma_{2l} + (g-h)\sigma_{1m}\sigma_{2m},$$

where

$$\sigma_{ik} = \sigma_i \cdot \mathbf{k},$$

σ_i is the Pauli spinor for particle i ($i=1,2$) in either the initial or the final system, and \hat{k} is a unit vector which takes the following three orthogonal directions \hat{n} , \hat{l} , or \hat{m} .

$\hat{n} = (\mathbf{k}_i \times \mathbf{k}_f) / |\mathbf{k}_i \times \mathbf{k}_f|$ is the normal of the scattering plane, \mathbf{k}_i and \mathbf{k}_f are the initial and final momenta for either particle 1 or particle 2, respectively, in the c.m. system.

$\hat{l} = (\mathbf{k}_i + \mathbf{k}_f) / |\mathbf{k}_i + \mathbf{k}_f|$. In the nonrelativistic case for scattering two particles of identical mass, \hat{l} is in the direction of final momentum in the laboratory system.

$\hat{m} = (\mathbf{k}_f - \mathbf{k}_i) / |\mathbf{k}_f - \mathbf{k}_i|$ is a unit vector perpendicular to both \hat{n} and \hat{l} , and the three directions are mutually perpendicular and form a right-handed coordinate system.

For a given interaction (i.e., pp , pn , or nn), the coefficients a , c , m , g , and h are the five complex (Wolfenstein) amplitudes (functions of E and θ^*) with names such as non-spin-flip, one-spin-flip, and double-spin-flip associated with them.